Journal of Aerosol Science 140 (2020) 105480

Contents lists available at ScienceDirect

Journal of Aerosol Science

journal homepage: http://www.elsevier.com/locate/jaerosci

Transient numerical simulation of airflow and fibrous particles in a human upper airway model

Morteza Kiasadegh [a], Homayoun Emdad [a], Goodarz Ahmadi [b], Omid Abouali [a,*]

[a] Shiraz University, Shiraz, Fars, Iran
[b] Clarkson University, Potsdam, NY, USA

ARTICLE INFO

Keywords:
Ellipsoidal fibers
Unsteady particle tracking
Eulerian-Lagrangian method
Human respiratory tract

ABSTRACT

In this study, the unsteady airflow field in a realistic model of human upper airways during the breathing cycle and the fibrous particle transport and deposition were investigated using the CFD method. An anatomically realistic model of airway passage including vestibule to the end of the trachea was constructed from the CT images of a 24-year-old healthy woman. Several user-defined functions (UDFs) were developed and incorporated into the discrete phase model (DPM) of ANSYS Fluent code and were used for the evaluation of ellipsoidal particle motion in transient airflows. The developed UDF was used to solve the coupled translational and rotational equations of motion of ellipsoidal fibers and to analyze their dispersion and deposition in the upper airways. The total and regional depositions for a range of fiber sizes were evaluated. The transient particle deposition fraction was compared with those obtained for the equivalent steady flow condition. In addition, the fraction of ellipsoidal fibers that penetrate the lower respiratory tract under cyclic breathing was calculated and compared with the steady flow simulation. The presented results showed that the steady simulation with an appropriate equivalent airflow rate can predict the total fibrous particle deposition during cyclic breathing with reasonable accuracy. The steady simulations, however, cannot properly predict the regional particle deposition under transient flows. In particular, the comparison between steady and transient penetration fraction reveals that the steady breathing model fails to accurately predict the penetration fraction of ellipsoidal fibers into the lower respiratory tract.

1. Introduction

During inhalation, airborne particulate pollutants can penetrate the human upper airway and enter the deep lung and potentially damage the sensitive tissues. The human nasal cavity is the first important protective line of defense for preventing exposure to suspended particulate matters. It is also known that the major-axis of the ellipsoidal particles is typically aligned with the flow direction and enables the fibrous particles to penetrate deeper into the lung (Tavakol, Ghahramani, Abouali, Yaghoubi, & Ahmadi, 2017; Tian & Ahmadi, 2013). That makes Asbestos, as well as, carbon and glass fibers more carcinogenic. Fibrous materials are found in many industrial applications due to their use as effective heat insulators (Zhou, Su, & Cheng, 2008). Ellipsoidal fibers that are inhaled and deposited in the human respiratory system can cause serious lung diseases including lung cancer and asbestosis (Fenoglio et al., 2011). Fibrous particles can also be used as novel carriers for targeted pulmonary drug delivery to combat various diseases. Thus,

* Corresponding author.
E-mail address: abouali@shirazu.ac.ir (O. Abouali).

https://doi.org/10.1016/j.jaerosci.2019.105480
Received 21 May 2019; Received in revised form 29 October 2019; Accepted 30 October 2019
Available online 6 November 2019

knowledge of fibrous particle transport and deposition in the human respiratory tract is of considerable importance.

In the last two decades, numerous experimental and numerical studies were carried out to investigate the deposition of spherical particle in the human upper airway (Abouali et al., 2012; Bahmanzadeh, Abouali, Faramarzi, & Ahmadi, 2015; Dong et al., 2018; Edgar, Matida, & Johnson, 2010; Farhadi Ghalati et al., 2012; Garcia, Tewksbury, Wong, & Kimbell, 2009; Ghahramani, Abouali, Emdad, & Ahmadi, 2014; Kelly, Asgharian, Kimbell, & Wong, 2004; Kesavanathan, Bascom, & Swift, 1998; Moghadas, Abouali, Faramarzi, & Ahmadi, 2011; Naseri, Abouali, & Ahamdi, 2017; Naseri, Abouali, Ghalati, & Ahmadi, 2014; Naseri, Shaghaghian, Abouali, & Ahamdi, 2017; Nikookar, Abouali, Eghtesad, Sadrizadeh, & Ahamdi, 2019; Shanley, Zamankhan, Ahmadi, Hopke, & Cheng, 2008; Smith, Cheng, & Yeh, 2001; Tavakoli, Abouali, Bagheri, Yazdi, & Ahmadi, 2012; Zamankhan et al., 2006; Zhang, Kleinstreuer, & Kim, 2002; Zhao, Feng, Bezerra, Wang, & Sperry, 2019; Zhou & Cheng, 2005). Ahmadi and Abouali (2017) have provided an extensive review of literature in related areas. Comparatively, less attention was given to transport and deposition of ellipsoidal fibers in the human respiratory system. Only a few experimental and numerical studies have been performed on the deposition of ellipsoidal fibers in a human airway replica. For example, Su and Cheng (2005) measured the deposition efficiency of carbon fibers in a human nasal model. Wang, Hopke, Ahmadi, Cheng, and Baronc (2008) experimentally investigated the effect of flow rate, particle aspect ratio and nasal geometry on the deposition pattern of fibrous particles in three human nasal cavities. Inthavong, Wen, Tian, and Tu (2008) studied numerically the deposition of ellipsoidal fibers in the left and right nasal cavity of an adult person using a simplified effective drag model. Tian et al. (2012) performed a computational study of fiber deposition in an idealized human lung airway. Transport and deposition of ellipsoidal fibers in the human upper airway were analyzed by Tian and Ahmadi (2013), where a multi-level asymmetric lung bifurcation model was used. They found that slender fibers tend to align themselves with the main flow stream during their flights. Feng and Kleinstruer (2013) numerically examined the deposition of ellipsoidal fibers in a model of the human respiratory system from the oral cavity to the 4th generation of the respiratory tract and compared their results with those for spherical particles. Dastan, Abouali, and Ahmadi (2014) evaluated the deposition of fibrous particles in three models of the human nasal cavity. They showed that the aerodynamic diameter is an appropriate parameter for correlating fiber deposition rates. Tavakol et al. (2017) reported the deposition fraction of ellipsoidal fibers in a realistic model of a human nasal cavity under laminar and turbulent airflow conditions. (Asgharian, Owen, Kuempel, & Jarabek, 2018) studied the deposition of inhaled elongate mineral particles in the respiratory tract based on dosimetry model simulations. They reported that the inhalability of elongated mineral particles is greater than that of spherical particles of the same mass or volume. Recently Farkas, Lizal, Elcner, Jedelsky, and Jicha (2019) simulated the deposition of fibers in an oro-pharyngeal-laryngeal-bronchial system at different flow rates and compared the results with the experimental data.

Although in most of the earlier studies, the transient nature of breathing was ignored due to the desire to reduce the computational cost, there have been some studies on spherical particles transport and deposition in cyclic airflows in human upper airway models. Häußermann, Bailey, Bailey, Etherington, and Youngman (2002) experimentally investigated the total deposition under constant airflow and cyclic human breathing patterns and reported that the total deposition for constant airflow is significantly higher than those for cyclic breathing. Shi, Kleinstreuer, and Zhang (2006) numerically simulated the regional and total nanoparticle depositions during cyclic airflow in the nasal cavity. They also showed that the effects of unsteady nature of the flow cannot be neglected. Grgic, Martin, and Finlay (2006) studied experimentally and numerically the deposition of particles in a human mouth throat model and reported that the deposition rates for unsteady airflow are higher than those of the equivalent steady flow condition. Using combined numerical and experimental approaches, Hörschler, Schröder, and Meinke (2010) studied the airflow fields in a model of human nasal cavity under steady and unsteady breathing. Recently, spherical particle transport and deposition in a nasal cavity under transient breathing condition was investigated by Bahmanzadeh, Abouali, and Ahmadi (2016). They reported the instantaneous deposition rate of particles in a single nasal passage during the inhalation phase of breathing. (Naseri et al., 2017) and (Naseri et al., 2017) performed a series of unsteady Lagrangian particle tracking and evaluated the deposition rate in healthy human upper airways. In this work, the time-dependent behavior of inhaled spherical particles and the transient particle deposition fractions for various regions of the human upper airway were evaluated and compared with those obtained for the equivalent steady flow assumption. They reported that there were noticeable differences in the predicted local deposition unsteady and equivalent steady flow simulations. Haghnegahdar, Zhao, and Feng (2019) investigated the transport, deposition, and resultant immune system response of the low-strain Influenza A Virus IAV laden droplets in a subject-specific human respiratory system. The hygroscopic growth and shrinkage behaviors of droplets were included and the corresponding droplet deposition fractions were simulated during both mouth and nasal steading breathings.

The above literature survey indicates that the regional depositions of elongated particles in a realistic model of the human upper airway from nostril to trachea under cyclic breathing conditions have not been studied. In the present study, the unsteady airflow field and the total and regional fibrous particle deposition in a realistic model of human upper airways extending from nostril to the end of trachea under steady and cyclic breathing conditions are investigated. The user-defined functions (UDFs) developed by Tavakol et al. (2017) were extended for application to unsteady simulations and were incorporated into the ANSYS Fluent software and were used to analyze the time-dependent behavior of ellipsoidal fiber under transient breathing condition. Comparisons of the total and regional fiber deposition under cyclic breathing conditions with those obtained from the equivalent steady flow condition showed that the steady simulation predicted the total deposition of ellipsoidal fibers in the upper respiratory tract with reasonable accuracy. The steady equivalent flow assumption, however, did not correctly predict the regional deposition rate of ellipsoidal fibers, as well as, the ellipsoidal fibers penetration rate.

2. Methods

2.1. Geometry

The 3D model of a human upper airway from nostril to the end of trachea of a healthy 24-year-old female volunteer, which was studied earlier by Farhadi Ghalati et al. (2012), Ghahramani et al. (2014) and Naseri, Abouali, Ghalati, and Ahmadi (2014, (Naseri et al., 2017), was used in this study. Fig. 1 shows the 3D view of the constructed airway model that was used in the present simulations. For mesh generation in the airway model, an unstructured grid with the Delaunay method was used. In addition, 6 prismatic boundary layer grids along the wall were used to more accurately resolve the near-wall flow and particle motions. For grid sensitivity study, different grids 3.7, 8.5 and 14.7 million cells were tested and it was found that a mesh with about 8,500,000 cells was sufficient for accurate simulations.

2.2. Boundary condition

In this study, the time-dependent airflow rate during cyclic breathing is assumed to be a sinusoidal function given as,

$$Q(t) = Q_{peak}\sin(2\pi ft) \tag{1}$$

where Q(t) is the time-depended airflow rate, Q_{peak} is the peak flow rate and f is the breathing frequency. Equation (1) was imposed as a boundary condition at the end of trachea.

The simulation was continued for three breathing cycles and it was found that the second and third cycle flow field results, such as velocity and pressure contours are quite similar. Therefore, the findings for the second breathing cycle are presented in the results section. For steady simulation, the equivalent mean flow rate during the inhalation phase of breathing is calculated as,

$$\overline{Q} = \frac{1}{2}\int_{t=0}^{t=2s} Q_{peak}\sin(2\pi ft)dt \tag{2}$$

Here a peak flow rate of 20 L/min and the breathing frequency of f = 0.25 HZ were assumed for the unsteady airflow simulation. Using Equation (2) in (1) leads to the equivalent mean flow rate of 12.8 L/min. The time variations of the boundary condition for cyclic breathing and its equivalent mean flow rate are shown in Fig. 2.

To investigate the flow time step sensitivity, three time steps of 0.01 s, 0.05 s and 0.25 were used in the simulations. It was found that the results for time steps of 0.01 s and 0.05 are nearly the same; therefore, the flow time step of 0.05 s was selected for the subsequent simulations. Time step sensitivity for the discretization of particle equation was also examined using time steps of $0.05\tau_p$, $0.1\tau_p$, and τ_p where τ_p is the particle relaxation time. It was found a time step of $0.1\tau_p$ was sufficient for accurate simulation of particle motion for both steady and unsteady (cyclic) breathing airflow conditions. Similar time step sensitivity was reported earlier by Dastan et al. (2013). The ellipsoidal particle relaxation time is given as:

$$\tau_p = \frac{4a^2\beta\rho^p}{\mu(\underset{\sim}{k}_{xx} + \underset{\sim}{k}_{yy} + \underset{\sim}{k}_{zz})} \tag{3}$$

where $\underset{\sim}{k}_{ii}$ is the element of the resistance tensor reported by Dastan et al. (2013). The relaxation times of the investigated fibers varied in the range of 0.004 s to 10^{-5} s.

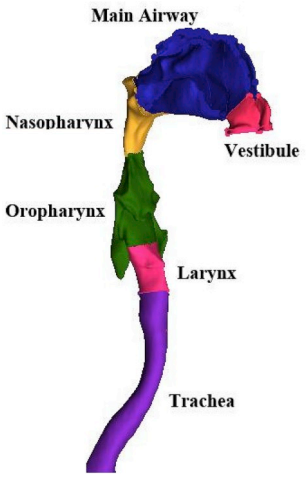

Fig. 1. The 3D model of reconstructed human upper airways.

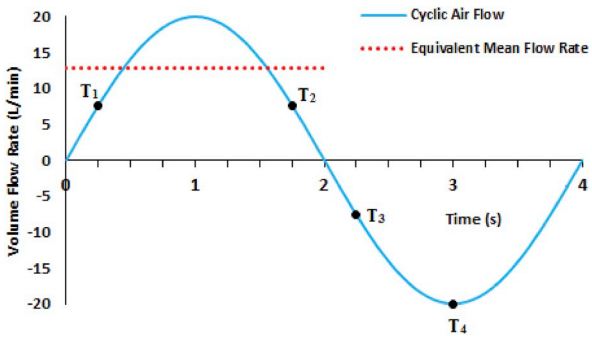

Fig. 2. The time-dependent sinusoidal breathing volume flow rate and the corresponding equivalent mean airflow rate.

Due to the unsteady nature of cyclic breathing, continuous particle injection is used during the inhalation phase. For each diameter and aspect ratio, 2230 fibrous particles were injected at each time step during the entire inhalation period. The sensitivity of the results to the number of injected particles was also studied. The number of injected particles was varied in the range of 1000–10000 and the deposition of particles was evaluated. A comparison of the findings showed that the predicted regional and total particle deposition becomes independent of the number of injected particles for samples equal to 2230 particles or larger.

An ellipsoidal fiber is assumed to enter the nostril with the local airflow velocity with its major axis oriented in the flow direction. The human respiratory system is covered with a layer of mucus. Therefore, particles stick to the wall upon contact, and the trapped wall boundary condition is used for particle-wall interaction. That is, it is assumed that a particle deposit on the wall of respiratory passage once it touches the wall.

3. Governing equation

3.1. Airflow field

The airflow field in the respiratory tract is assumed to be unsteady, laminar and incompressible with constant viscosity. Accordingly, the continuity and Navier-Stokes equations are given as,

$$\nabla \cdot \mathbf{u} = 0 \tag{4}$$

$$\frac{\partial \mathbf{u}}{\partial t} + \mathbf{u} \cdot \nabla \mathbf{u} = -\frac{\nabla p}{\rho} + \nu \nabla^2 \mathbf{u} \tag{5}$$

where $\mathbf{u}$, p, ρ and ν are, respectively, the airflow velocity vector, the pressure, the air density, and the air kinematic viscosity.

3.2. Fiber motion

The translation motion of a particle of arbitrary shape is governed by,

$$\frac{d}{dt}(m_p \mathbf{v}_p) = \sum \mathbf{F} \tag{6}$$

Here m_p,$\mathbf{v}_p$ and $\mathbf{F}$ are, respectively, the particle mass, the velocity vector of particle mass center, and the force vector acting on the particle. According to a survey conducted by Ouchene et al., 2015, only hydrodynamic drag and gravitational forces have a significant influence on the studied particle motion and the other forces have been neglected.

The rotational motion of the ellipsoidal particle is governed by the balance of angular momentum. That is,

$$\frac{d}{dt}(\mathbf{I}_p \cdot \boldsymbol{\omega}_p) = \sum \mathbf{T} \tag{7}$$

Here $\mathbf{I}_p$, $\boldsymbol{\omega}_p$ and $\mathbf{T}$ are, respectively, the moment of inertia, the particle angular velocity and the hydrodynamic torque acting on the particle. The details of the equations of motion of ellipsoidal fibers and the conditions for ellipsoidal particle deposition were reported, respectively, by Tian and Ahmadi (2013) and (Fan and Ahmadi, 1995a), (Fan and Ahmadi, 1995b). Therefore, the details are not repeated here for the sake of brevity.

3.3. Numerical setup

To simulate the airflow field in the respiratory tract, the ANSYS Fluent (Version 15) commercial software with the SIMPLE algorithm was used. The Lagrangian trajectory analysis approach in conjunction with the balance of angular momentum was used to

solve the fiber equations of motion. Since the ANSYS Fluent software does not have the capability of solving the coupled equations of the balance of linear and angular momentum of ellipsoidal fibers, the UDFs developed by Tavakol et al. (2017) were upgraded for solving the equation of motion of ellipsoidal fibers in transient flows. During the inhalation phase of breathing, ellipsoidal fibers with density of 1000 kg/m^3, minor axis radius of 1, 3, 5, 10 μm and aspect ratio of 2, 10 and 25 were injected continuously at the nostril of the computational model of the airway, and their corresponding trajectories and orientations were analyzed.

4. Results

4.1. Streamlines and velocity field

Samples airflow streamlines and velocity contours at different times in the breathing cycle as marked in Fig. 2 are shown in Fig. 3. At times of 0.25, 1.75, and 2.25 s from the start of the inhalation period, the magnitude of airflow rate is 7.65 L/min. Fig. 3 shows that the airflow fields at times of 0.25 and 1.75 s that are both in the inhalation phase are roughly the same, with small differences in the larynx area due to the influence of the acceleration and deceleration of airflow. At t = 2.25s, however, the airflow field is quite different as this case is in the exhalation phase of the breathing. The maximum velocity is about 9.4 m/s at t = 3s during the peak of the exhalation phase. The peak airflow velocity at t = 1s during the inhalation is 9.411. (The velocity contours at t = 1s is not shown for the sake of brevity.) During the inhalation, a high-speed laryngeal jet forms in the larynx region and in the exhalation phase a low-speed jet is generated towards the nasopharynx region because of the sharp contraction of the pharynx. The effect of these two jets on particle deposition is further examined in the following sections.

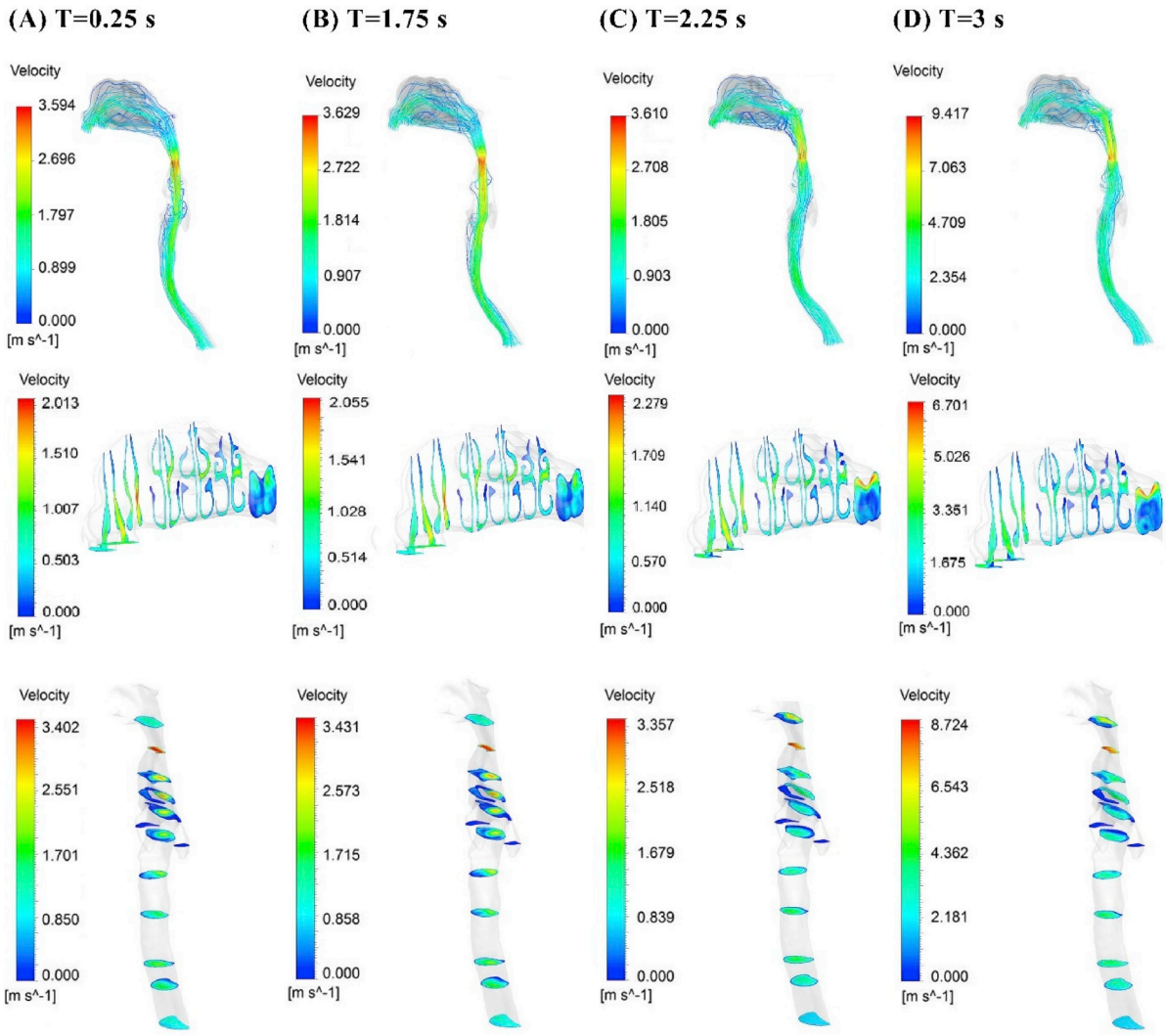

Fig. 3. Time evolution of airflow streamlines and velocity contours at four representative time instants.

4.2. Comparison of deposition fraction of steady and unsteady flow simulations

Naseri et al. (2017) showed that the steady flow simulation with properly selected effective velocity leads to a total deposition fraction of spherical particles in the upper airways that is comparable to that obtained under cyclic breathing. In this study, a similar comparison for fiber inhalation is performed. The total deposition fraction (TDF) of particles is defined as:

$$TDF(\%) = \frac{N_d}{N_{total}} \times 100 \tag{8}$$

where N_d is the number of particles deposited in the airway and N_{total} is the total number of particles inhaled through nostrils.

The comparisons of the predicted deposition rates for cyclic breathing with a peak inspiratory flow rate (PIF) of 20 L/min with those obtained under the equivalent steady flow rate of 12.8 L/min for fibrous particles with an aspect ratio of 2, 10 and 25, and a minor axis radius of 1, 3, 5, 10 and 15 μm are shown in Fig. 4. It is seen that as the aspect ratio, as well as, the semi-minor axis radius of the ellipsoidal fibers increases, the total deposition rates for both steady and unsteady simulations increase and levels off for large fiber radius. Fig. 4 also shows that the predicted total fiber deposition for steady flow is comparable with those evaluated under cyclic breathing. It is also seen that for the smallest size of particles with the same aspect ratio, the total deposition of the steady simulation is lower than the cyclic breathing. This is because the instantaneous airflow rate during the inhalation phase is greater than the equivalent mean flow rate for about 60% of the time. Therefore, the impaction parameter for a fine particle in the unsteady flow is higher in comparison with the steady flow case in most of the inhalation cycle. However, the large particle deposition under the cyclic flow is slightly lower than those predicted by the equivalent steady flow simulation. This is because, for this range of the particle sizes, the impaction parameter in the steady simulation is already sufficiently high for particle deposition. For the unsteady simulation, however, the impaction parameter magnitude in the low volume flow rate durations is not high enough and therefore the chance for deposition decreases in the time duration that the flow rate is small.

The maximum absolute difference of 15.18% between total deposition fractions obtained by unsteady and steady simulations is seen for ellipsoidal fibers with semi-minor axis length of 5 μm and the aspect ratio of 2, and the maximum relative difference of 60.61% between total deposition fractions obtained by unsteady and steady simulations is for ellipsoidal fibers with semi-minor axis length of 3 μm and the aspect ratio of 2.

4.3. Comparison of deposition, penetration and exhalation fractions of steady and unsteady flow simulations

In this section fibrous particle deposition and penetration fractions for steady and cyclic breathing conditions are studied and compared. In addition, the particle exhalation fraction during the exhalation phase of cyclic breathing is also studied. The penetration fraction PF is defined as,

$$PF(\%) = \frac{N_p}{N_{Total}} \times 100 \tag{9}$$

where N_P is the number of particles that passes through the trachea outlet and penetrate into the first lung generation. It was assumed that the particles that pass through the outlet are deposited in the lung and no particle will re-enter the upper airways from the computational domain outlet during the exhalation phase. Since there is no expiration phase in the steady flow model, no particles are breathed out from the entrance of the airways. Therefore, particles that enter the respiratory tract either deposit or penetrate into the deep lung regions. However, in the transient simulation during cyclic breathing, some particles are breathed out during the exhalation phase. The particle exhalation fraction (EF) is defined as,

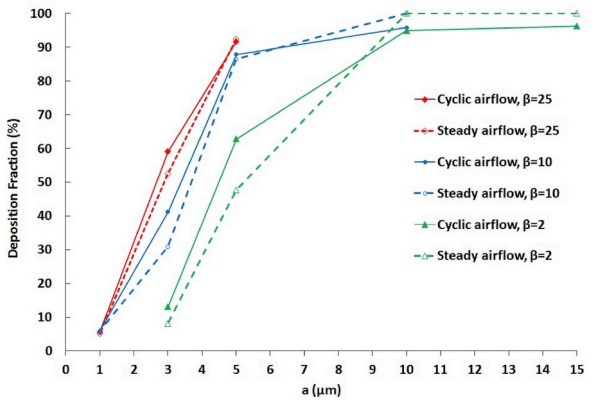

Fig. 4. Comparison of total deposition fractions obtained by unsteady and steady simulations.

$$EF(\%) = \frac{N_E}{N_{Total}} \times 100 \tag{10}$$

where N_E is the number of particles that is exhaled via nostrils during the exhalation phase of breathing.

Fig. 5 compares the penetration fraction, exhalation fraction and the total deposition fraction of fibrous particles for transient and steady simulations. As expected, increasing particle size and aspect ratio leads to an increase of the total deposition rate and decrease of penetration. An important point to mention is that the penetration fractions of steady and unsteady simulations show large differences. Clearly, the steady simulation assumes all particles that are not deposited penetrate into the lower lung, while during the cyclic breathing a fraction of suspended particles is exhaled from the nostrils, and the rest penetrate into the deep lung. This leads to the maximum relative difference of penetration fractions of 236% between cyclic and steady breathing conditions for ellipsoidal fibers with $a = 5\ \mu m$ and $\beta = 10$. The minimum relative difference of penetration fraction of 23% between cyclic and steady simulations is seen for particles with $a = 1\ \mu m$, $\beta = 10$.

In the transient simulation, when the aspect ratio increases five times for a fixed fiber minor axis radius, the penetration fraction is reduced by 26.28% and if the fiber radius increases fivefold for a fixed β, the penetration fraction is reduced by 72.36%. This indicates that the effect of increasing the fiber radius on fiber penetration is much larger than the effect of increasing the aspect ratio. This is as expected as the volume (mass) of an ellipsoid is proportional to βa^3.

As expected, the steady simulation does not account for exhalation and the exhalation fraction would be zero. However, during the exhalation phase, a significant fraction of particles exhales from the airway. Fig. 5 shows that for the cyclic breathing, about 7–18 percent of the ellipsoidal fibers are exhaled from the nostrils. The exhalation fraction increases as the fiber radius and aspect ratio decrease.

Comparing Figs. 4 and 5 suggests that the results of the steady simulation are reasonable only for the total deposition. The steady flow simulation, however, cannot properly evaluate the particle penetration into the deep lung. Evaluation of penetration rates of ellipsoidal fibers into the lung is of significant interest for health hazard and exposure assessments, which has to be evaluated using the unsteady breathing model. As noted before, the majority of earlier studies were limited to steady simulation, and therefore, their penetration estimations are probably inaccurate.

4.4. Comparison of regional deposition for steady and unsteady simulation

Understanding the regional particle deposition is important for targeted drug delivery to specific areas of pulmonary track and also for assessing the hot zones for pollutant deposition. In this section, the regional particle deposition fraction is defined as the ratio of the number of deposited particles in the target area to the total number of particles entering the respiratory tract during the inhalation phase. The regional deposition fractions in the respiratory tract during cyclic breathing with the PIF of 20 L/min and the corresponding steady flow rate of 12.8 L/min are evaluated and the results are shown in Fig. 6. For both steady and unsteady respiration, this figure shows that the majority of particles deposit in the nasal valve and larynx, and a small fraction of particles deposit in the pharynx and trachea.

As the particle size decreases ($a = 3\ \mu m$, $\beta = 2$), the chance for particle deposition in all regions decreases and there are no

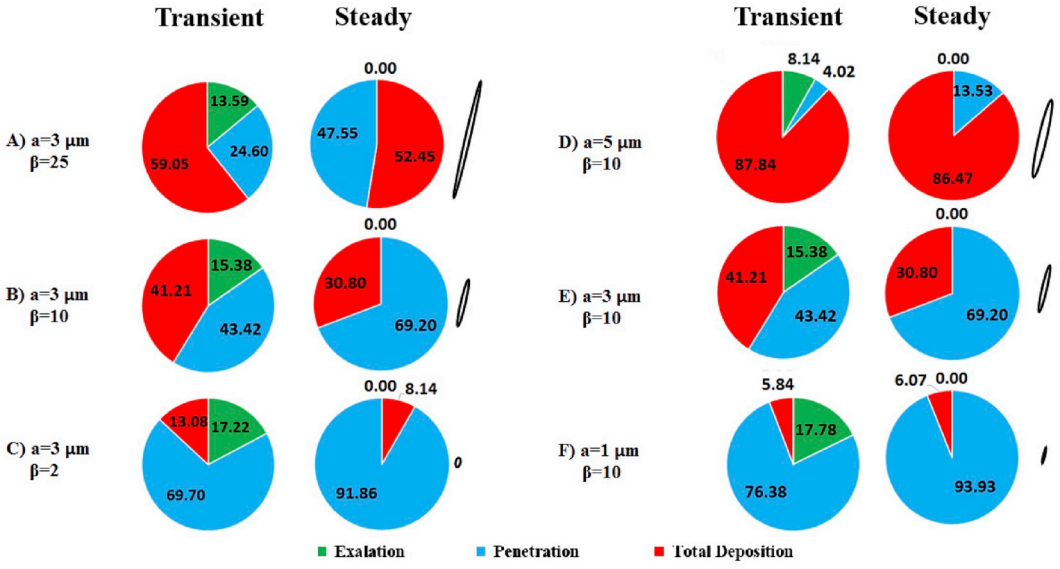

Fig. 5. Comparison of deposition, penetration and exhalation fractions of ellipsoidal fibers for cyclic breathing and its equivalent steady breathing simulations.

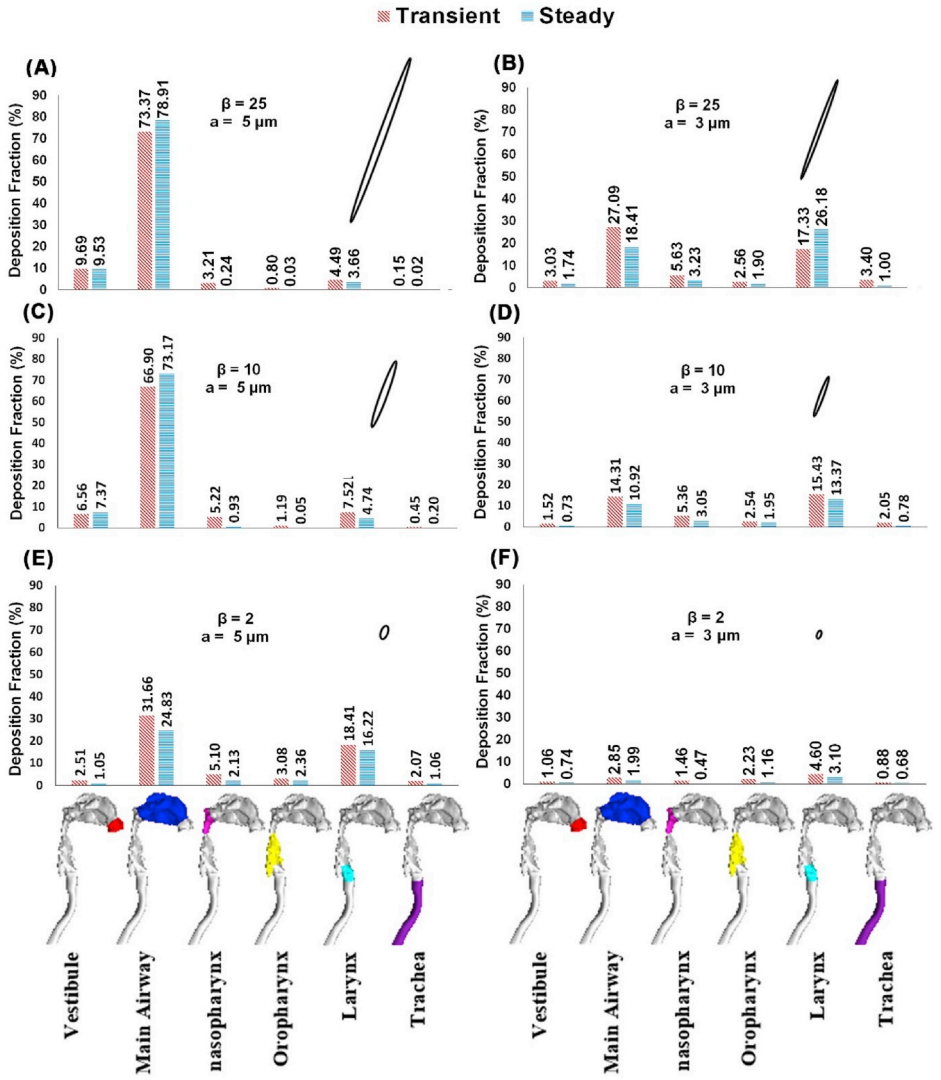

Fig. 6. Comparison of the regional deposition fractions for cyclic breathing patterns and its equivalent steady flow simulation for different particle sizes and aspect ratios.

deposition hot spots. The maximum deposition in the larynx area occurs for medium-sized particles ($a = 3\,\mu m$, $\beta = 25$ and $a = 5\,\mu m$, $\beta = 2$), which is followed by the fibers with $a = 3\,\mu m$, $\beta = 10$. A comparable fraction of these size ellipsoidal fibers also deposits in the main airway.

The mechanism for high deposition fractions of large and medium-sized ellipsoidal fibers in the nasal cavity is the inertial impaction in the narrow and twisted airway passages in this region. In addition, some particles that penetrated through the nasal passages during the inhalation phase could deposit in this area during the exhalation phase. It is also noteworthy that the jet flow formation in the pharynx increases the particle momentum and thus the probability of particle deposition increases. This is perhaps the reason for the fairly high deposition fraction of medium-sized particles seen in Fig. 6. The trachea, however, behaves as a vertical tube with no twist or jet formation; therefore, the particle deposition in the trachea area is low for both steady inhalation and unsteady breathing.

Comparison of the regional fiber depositions for steady and unsteady flow simulations indicates that the steady flow analysis slightly overestimates the deposition fraction of large particles in the vestibule, main airway areas, and this trend is reversed in lower regions of the respiratory tract. As noted before, in a transient simulation, during certain time periods, the flow rate is low and thus the particle inertia is insufficient for their deposition in the nasal cavity; therefore, they could penetrate into the lower regions of the upper airway and have the chance of depositing when the breathing flow rate increases. In the steady flow analysis, the flow rate is constant and the inertia of all large particles is sufficiently high for their deposition in the nasal cavity with the impaction mechanism.

For smaller particle sizes the deposition fractions in the vestibule, main airway, and nasopharynx regions in the steady simulation are less than that of the unsteady analysis. The reason is for smaller particles under steady breathing condition, the corresponding

impact parameter is less than the threshold required for their deposition; therefore, only a small fraction of particles are deposited in these areas. In the unsteady breathing condition, during the time interval of 0.44–1.66 s, the airflow rate is larger than the equivalent steady inhalation; therefore, the fractions of impaction induced deposited particles in the vestibule and the main airway become larger than those predicted by the steady simulation.

In contrast to the upper region, the amount of medium-sized particle deposition predicted by the cyclic breathing in the lower part of the upper respiratory tract is less than that obtained by the steady flow assumption. This is because for the cyclic breathing a smaller number of particles reach the lower parts of the airway and therefore the probability of the deposition is lower.

The maximum absolute differences for the regional depositions for steady and unsteady simulations occur in the main airway of the nasal cavity and is 10.6% for ellipsoidal fibers with an aspect ratio of 25 and minor axis radius of 3 μm. The relative differences, however, can be quite high and occur for regions that the deposition fraction is very low. The relative differences can reach to 210.6 percent for regional deposition of ellipsoidal fibers with $\beta = 2$ and $a = 3$ μm in the nasopharynx region.

Fig. 6 also shows that the deposition of thicker ellipsoidal fibers in the nasal cavity is more than the slender ellipsoidal fibers, which is consistent with the earlier findings that slender high aspect ratio ellipsoidal fibers can more easily penetrate through the nasal cavity (Tavakol et al., 2017).

4.5. Particle deposition pattern

The spatial deposition patterns of ellipsoidal fibers with different aspect ratios under both cyclic and the equivalent steady flow conditions are evaluated and the results are presented and discussed in this section. For ellipsoidal fibers with the 3 μm minor axis radius, Fig. 7 shows the influence of aspect ratio on the spatial distribution of particle in the upper airways as predicted by the transient and steady simulations. To emphasize the important effects of transient breathing, the blue and red dots in this figure represent the location of deposited particles, respectively, in inhalation and exhalation phases. The black dots identify the particles that are captured in the steady simulations. The importance of fiber aspect ratio on the spatial distribution pattern of particle deposition can be clearly

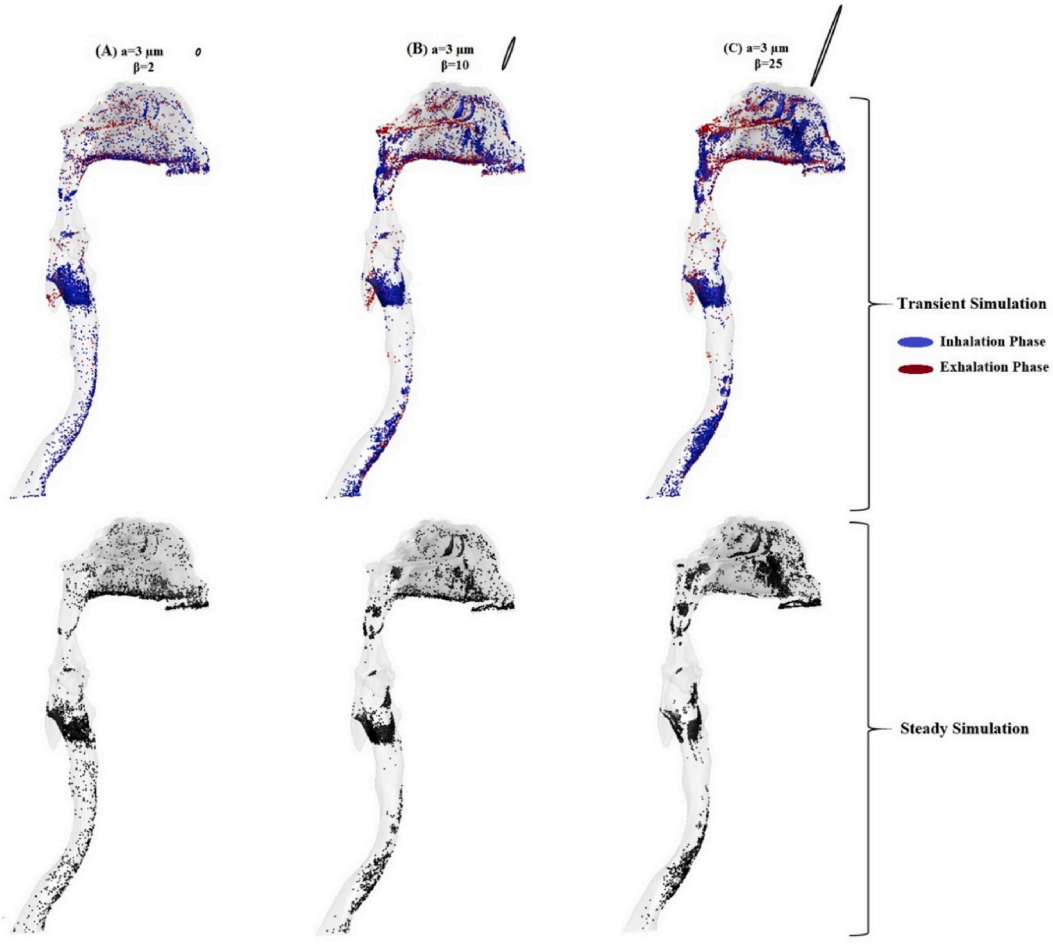

Fig. 7. Comparison of deposition patterns of 3 μm fiber and different aspect ratios as predicted by the cyclic breathing with the equivalent steady breathing simulations.

seen in Fig. 7. This figure shows that as the fiber aspect ratio increases, the fiber deposition rate increases especially in the nasal valve area. During the inhalation phase of unsteady breathing, a significant number of particles are also captured in the nasopharynx and main airway. In addition, a number of ellipsoidal fibers deposit in the lower part of the nasal valve region due to the sedimentation mechanism.

During the exhalation phase of breathing, the ellipsoidal fibers deposit in the main nasal airway and olfactory regions (bands of red dots), the amount of which increases sharply with the fiber aspect ratio. These regional depositions are absent during the inhalation phase (unsteady or steady) breathing. In addition, a significant percentage of particles deposit in the lower part of main airway. This occurs in the initial time interval of the exhalation phase that the airflow rate is low, and suspended particles deposit due to sedimentation. It is also observed that the ellipsoidal fibers deposition in the nasopharynx region increases during the exhalation phase due to jet flow in this region that increases the inertia-impaction parameter of particles.

The spatial deposition pattern of ellipsoidal fibers with a fixed aspect ratio $\beta = 10$ and various radii are presented in Fig. 8. This figure shows that fine ellipsoidal fibers with a minor axis radius less or equal 5 μm deposit in all parts of the airway model, but larger ellipsoidal fibers with radii of 10 and 15 μm are mostly captured in the frontal part of the nasal airway. The highest amount of particle deposition in the trachea occurs for the ellipsoidal fibers with the 3 μm radius.

Comparisons of the inhalation and exhalation deposition patterns in Fig. 8 show that the deposition of 3 and 5 μm ellipsoidal fibers during the exhalation phase is higher than the other sizes. The 3 and 5 μm ellipsoidal fibers are deposited in the entire airway, which indicates that they have penetrated into the lower part of the airway and have the chance to deposit during the exhalation phase. It can also be observed that another noticeable amount of particle deposition during the exhalation phase occurs on the floor of the nasal passage before these particles enter the vestibule, which is due to the relatively low airflow velocity in this region.

The time variations of spatial deposition pattern of 5 μm ellipsoidal fibers with an aspect ratio of 10 are shown in Fig. 9. It is seen that, up to the time instance of 0.25 s, small fractions of particles are deposited in the lower part of nasal main airway and the larynx regions. As time increases, the ellipsoidal fibers deposition in the nasal valve and larynx regions increases. The spatial deposition pattern at $t = 0.75$ s is similar to that in the time instance of 1.75 s but differs from that of the exhalation phase. Fig. 9 clearly indicates that a significant number of particles are captured during the exhalation phase in the areas that are not hot spots for particle deposition during the inhalation phase of the breathing cycle.

5. Time-dependent features of fiber deposition

To more accurately evaluate the transient motion of fibrous particles their behavior as a function of time is examined in detail in this section. For ellipsoidal fibers of different sizes and aspect ratios at a respiratory cycle with PIF of 20 L per minute, the transient particle deposition fraction for each time interval of 0.05 s is calculated, and the results are shown in Fig. 10. In the right column of Fig. 10, the enlarged views of the graph for deposition in the exhalation phase are shown. The transient particle deposition fraction (percentage) is defined as,

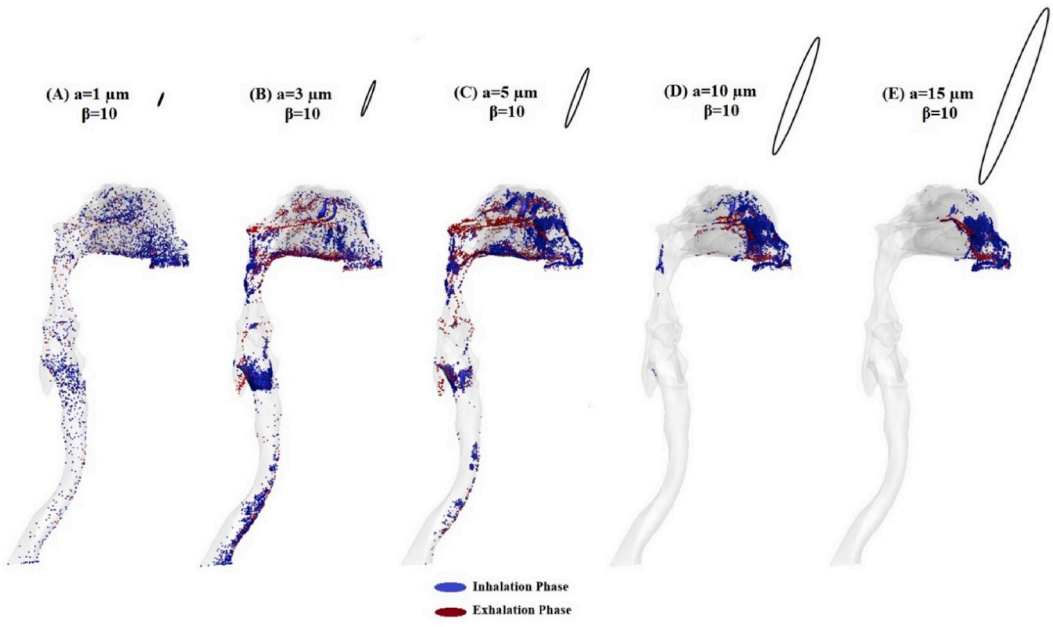

Fig. 8. Deposition patterns of ellipsoidal fibers with the $\boldsymbol{\beta} = 10$ and different radii during the inhalation and exhalation of unsteady breathing.

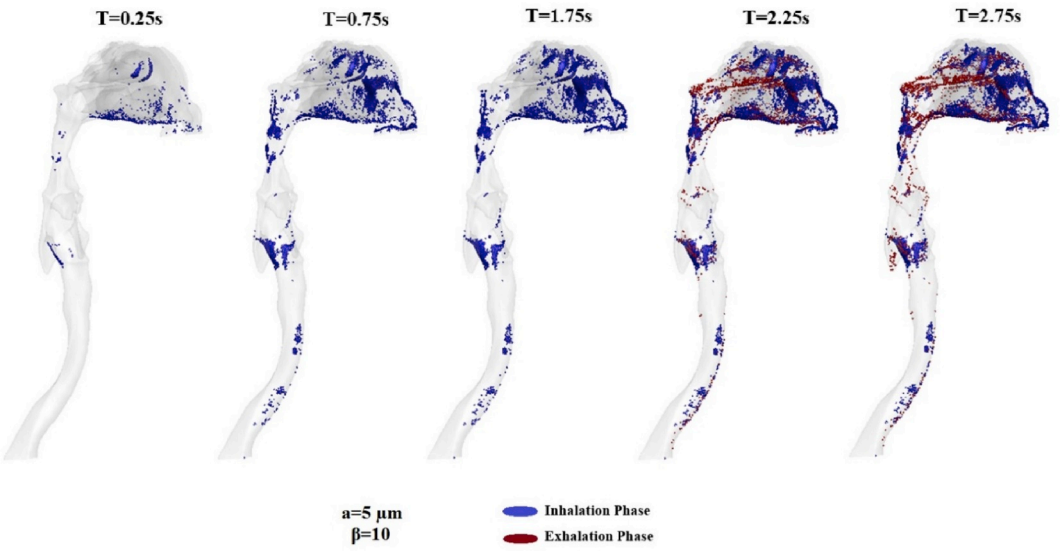

Fig. 9. Time variations of spatial deposition pattern of ellipsoidal fibers with a = 5 μm and **β** = 10.

$$\mathrm{TPD}(\%) = \frac{N_{t-i}}{N_{\mathrm{Total}}} \times 100 \tag{11}$$

where $N_{t\text{-}i}$ is the number of deposited particles in a time interval. For a fixed aspect ratio, Fig. 10(A), 10(B) and 10(C) show that the increase of the fiber minor radius generally leads to the increase of the deposition fraction, except for certain time intervals. The influence of the fiber aspect ratio effect on the transient fiber deposition is shown in Fig. 10(D). It is seen that the transient particle deposition increases as the fiber aspect ratio increases, except at certain time intervals. Clearly as fiber size increases due to the increase in its radius or aspect ratio, so does its impaction parameter that leads to the increased deposition.

For small ellipsoidal fibers, the maximum transient deposition occurs in the time range of 0.9–1.1 s when the inhalation flow rate is near its maximum. This is because at the beginning of the inhalation phase when the airflow velocity is low, the inertia of small particles is not sufficiently high for their deposition; therefore, only a few fine particles deposit. With an increase in the flow rate, these particles obtain sufficient inertia for deposition. Then in the deceleration phase of breathing, the flow rate decreases and the transient fine particle deposition fraction decreases again.

It can be observed from Fig. 10 that, for large particles, the transient deposition fraction increases sharply and reaches its maximum value in the time range of 0.2–0.5 s. In addition, as the particle size increases, the peak deposition occurs at an earlier time. This is because the inertia of large particles entering the respiratory system in the initial time intervals (0–0.2 s) is not sufficiently large for their deposition on the wall; hence, most of these particles remain suspended in the airway. But in the subsequent time intervals, the inhalation airflow rate increases and these suspended particles in addition to the particles entering the nostrils acquired sufficient inertia for deposition, causing a rapid increase in the transient deposition fraction. After the sharp increase to the peak value, the deposition fraction remains roughly constant. This is because the particle velocity is at the level that is sufficient for deposition in the next time steps shortly before the end of the inhalation phase. As long as the flow rate is not less than the required level for deposition, the deposition fraction remains roughly constant and is almost equal to the ratio of the number of particles injected in a single time step to the total number of inhaled particles. The same pattern was also observed for spherical particles in the earlier study of Naseri et al. (2017). Fig. 10 also shows that the constant deposition range for larger particles is greater than those for smaller particles. This is because the critical flow rate for large particles is lower than that for fine particles.

A small local peak deposition in the time interval between 1.9 and 2.1 is seen in Fig. 10, which is more visible for larger particles. This time interval is at the end of the inhalation phase that the airflow rate is quite low to the extent that large particles can deposit on the walls of the respiratory tract due to the sedimentation mechanism.

Fig. 10(A) shows that the maximum fiber deposition with a semi-minor axis length of 10 μm and an aspect ratio of 2 is greater than that of a 15 μm fiber with an aspect ratio of 2. This is because more 15 μm ellipsoidal fibers are deposited at the earlier times.

Fig. 10 also indicates that an additional local increase in deposition occurring in the time interval of 2.2–2.4 s in the exhalation phase due to the deposition of a number of suspended particles on the walls of the airways with increasing fluid velocity. The group of enlarged figures on the right of Fig. 10 reveals that the ellipsoidal fibers of moderate size (with a radius larger than 1 μm) have a maximum deposition fraction during the exhalation phase.

Another important time-dependent behavior is the transient penetration of ellipsoidal fibers into the lung region that is shown in Fig. 11. The transient penetration fraction is defined as the ratio of the number of particles that passes through the trachea outlet into the lower lung in each time interval to the number of total inhaled particles during inhalation. As expected, Fig. 11(A), 11(B) and 11(C) show that the particle penetration generally reduces by increasing the fiber radius and aspect ratio. For example, all 10 μm ellipsoidal

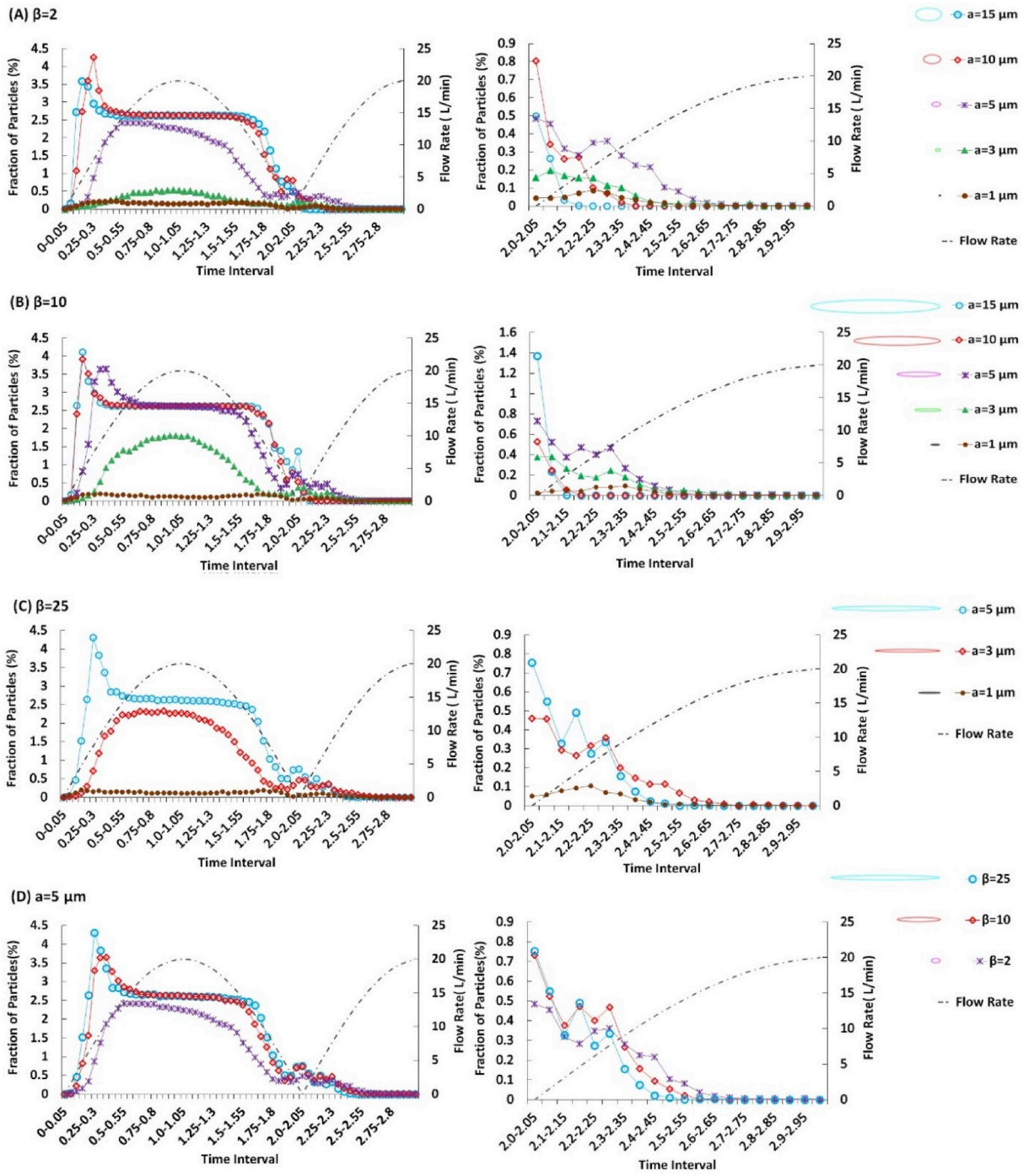

Fig. 10. Variation of deposition fractions at various time intervals under the cyclic breathing for different fiber sizes and aspect ratios.

fibers with an aspect ratio of 10 are deposited in the upper airways with no penetration into the lower lung, but the 3 μm ellipsoidal fibers with an aspect ratio of 2 penetrate through at all time intervals, except the first 0.25 s.

It is seen that there is no penetration in the time duration of 0–0.25 s at the start of inhalation for all fiber sizes and aspect ratios. This is because the airflow velocity is low and the particles do not reach the end of the trachea in this time duration. Fig. 11 also shows that in the time interval of 0.3–0.45 s the peak penetration fraction occurs. After 0.45 s, the inertia of the particles increases with the increase of the inhalation rate and thus the penetration of the particles decreases due to the deposition of fiber by impaction mechanism.

The penetrations of 3 μm ellipsoidal fibers with different aspect ratios are shown in Fig. 11(D). It is seen that the penetration

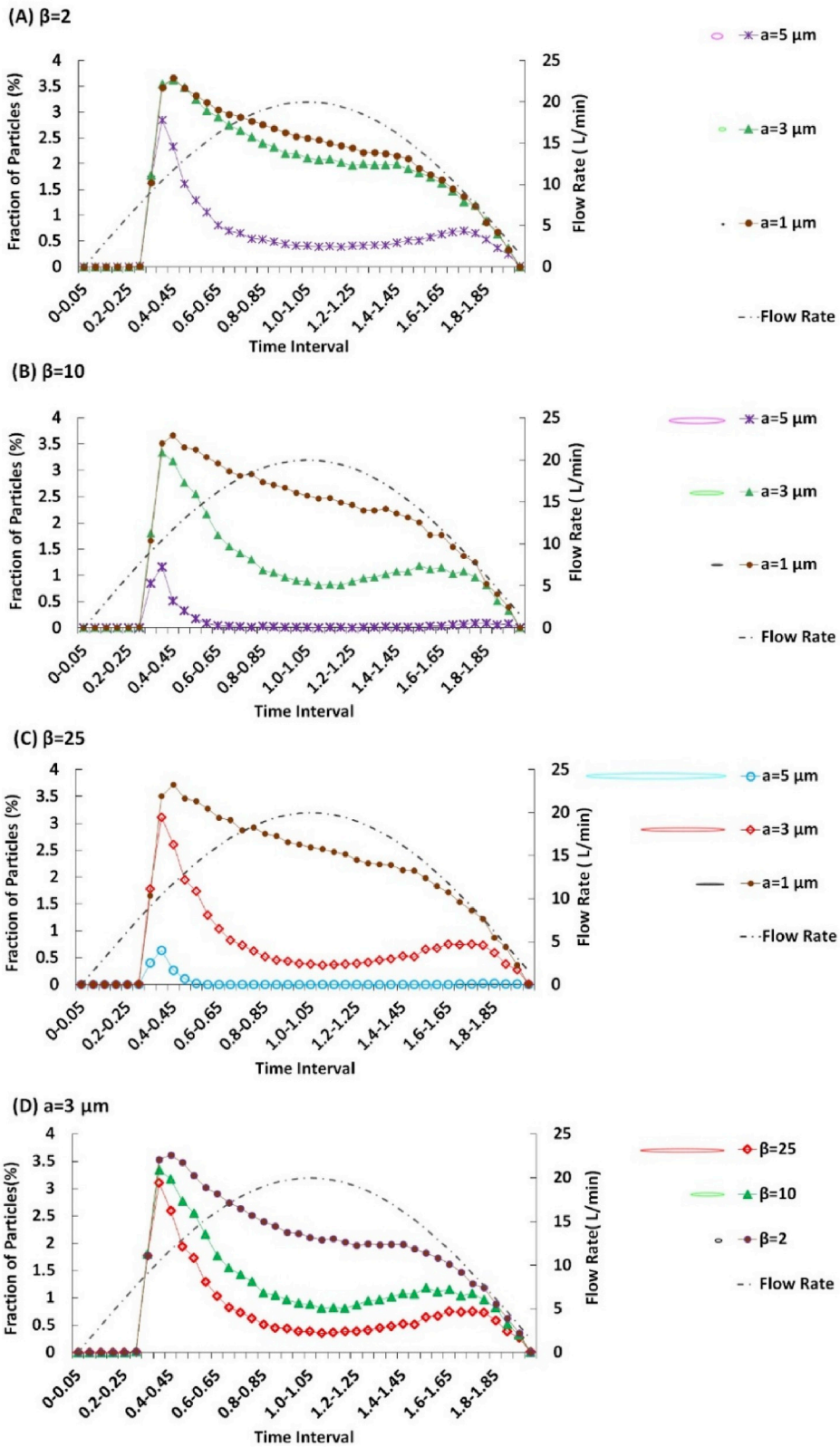

Fig. 11. Variation of penetration fraction at various time intervals of cyclic breathing for different fiber sizes.

fraction decreases with the increase of aspect ratio so that the penetration fraction of ellipsoidal fibers with an aspect ratio of 25 is lower than 0.5%.

For particles of moderate size ($\beta = 2$ and $a = 5$ μm, $\beta = 10$ and $a = 3$ μm, $\beta = 25$ and $a = 3$ μm), the penetration fraction increases in the time interval of 1.6–1.8 s, which is due to decrease in particle deposition by impaction and sedimentation. In general, the presented results show that the upper respiratory system can only filter out very large ellipsoidal fibers but small and medium-sized fibrous

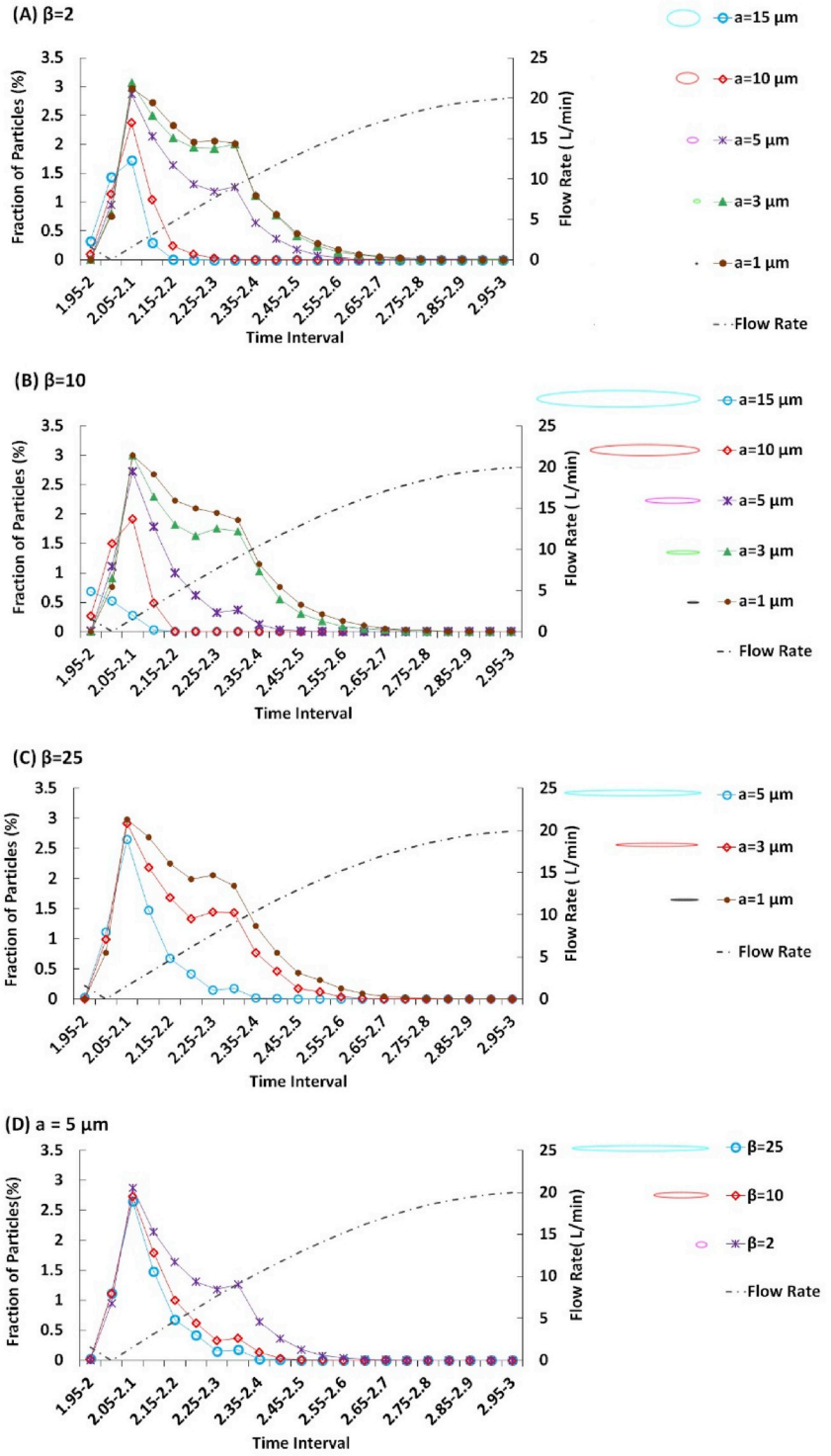

Fig. 12. Variation of exhalation fraction at various time intervals of cyclic breathing for various particle sizes.

particles can penetrate into the lung area and cause serious health issues.

One major advantage of the cyclic airflow simulations over the steady analysis is accounting for flow and particle deposition during the exhalation phase of breathing. In particular, information on the fraction of exhaled particles is provided. Fig. 12 shows the time variation of the number of particles exhaled from the nostril for ellipsoidal fibers with various radii and aspect ratios. This figure indicates that a fraction of suspended particles in the upper airway is ejected out of the nostril during the exhalation phase by the reversal of the airflow direction. When the airflow changes from inhalation to exhalation, particles that have not penetrated into the deeper lung move towards the nasal passage. With the increased flow velocity in the exhalation phase large ellipsoidal fibers deposit in the respiratory tract, but the small particles pass through the airways and exhale from the nostril. Exhaling small ellipsoidal fibers continues up to about 0.75 s after the beginning of the exhalation phase, but for large particles, the process ends at about 0.3 s after the start of the exhalation phase. Fig. 12 also shows that the peak exhalation fraction for all fiber sizes occurs in the time interval of 2.05–2.1 s. In addition, in the time interval of 2.3–2.35 s, the fraction of exhaled small ellipsoidal fibers shows a mild local peak.

6. Limitation of this study

In this computational study, several simplifying assumptions have been made that are summarized in this section. Some of these assumptions could be revisited and relaxed in future studies. Some of these key simplifications and limitations of the present study are:

- The breathing airflow profile was assumed to be a sinusoidal function. While this is a reasonable approximation for the breathing cycle, it is possible to use a measured breathing airflow profile that deviates somewhat from the sinusoidal profile in order to assess its significance on the transient particle deposition fraction.
- The present studied was the nasal breathing conditions and the effect of the oral cavity on the transient particle deposition was not considered.
- At the inlet, it was assumed that the ellipsoidal particles enter the nostril with their major axis aligned with the local flow. Preliminary performed simulations (not shown here for the sack of brevity) showed that the effect of variation in the initial orientation of fiber is negligibly small. A more detail study of the influence of variation of ellipsoidal fibers orientation, velocity, and angular velocity, however, are left for a future study.
- It was assumed that the air is dilute and a one-way coupled model is used. That is the airflow carries the particles but the influence of the particles on the airflow is ignored.
- The study assumed that the particle concentration is low and the inter-particle collisions and the interactions of particles with each other are neglected.

7. Conclusions

In this study, the transient transport and deposition of ellipsoidal fibers in a realistic model of the human upper airways for a full breathing cycle was numerically simulated. The corresponding total and region deposition fractions, as well as, the penetration and exhalation of ellipsoidal fibers of different radii and aspect ratios were evaluated and discussed. Attention was also given to the comparison of features of fiber deposition under cyclic breathing simulation and its equivalent steady airflow analysis. In particular, the accuracy of steady simulation in predicting the fiber deposition fraction and penetration rates was evaluated. Based on the presented results, the following conclusions were drawn:

1. Examination of total particle deposition predicted with steady and transient simulations showed that the steady simulation with an equivalent flow rate (average of the inhalation phase) was able to predict the total deposition of ellipsoidal fibers in the upper respiratory tract and trachea with reasonable accuracy.
2. Comparisons of the particle penetration rate showed significant differences between steady and cyclic simulations. In particular, the steady simulation over predicted the penetration fraction of ellipsoidal fibers as it ignores the revised airflow and the associated particle deposition during the exhalation phase of the breathing. The absolute difference was as high as 22.7%. Therefore, the use of steady simulation for the prediction of fiber penetration fraction into the deep lung is not appropriate.
3. Comparison of the regional fiber depositions for steady and unsteady flow simulations indicates that the steady flow analysis slightly overestimates the deposition fraction of large particles in the vestibule and main airway areas, and this trend is reversed in lower regions of the respiratory tract. In contrast to the nasal cavity, the medium-sized particle depositions predicted by the cyclic breathing in the lower part of the airway are less than those obtained by the steady simulation. For smaller particle sizes the deposition fractions in the vestibule, main airway, and nasopharynx regions in the steady simulation are less than those of the unsteady analysis. This observation suggests that in cases where the local depositions of the deposited particle are important, such as targeted drug delivery applications, the use of transient simulations is recommended.
4. The simulation showed that significant fractions of particles in the size range of $3\ \mu m \leq a \leq 15\ \mu m$, $2 \leq \beta \leq 25$ were deposited during the exhalation phase of breathing. The minimum exhalation fraction through the nostril was 7.5% for ellipsoidal fibers with $a = 5\ \mu m$ and $\beta = 10$. The maximum exhalation fraction was 18 percent for ellipsoidal fibers with $a = 1\ \mu m$ and $\beta = 10$. The simulation results indicated that a significant number of ellipsoidal fibers that were captured during the exhalation phase were deposited in areas that were not a hot zone for particle capture during the inhalation phase.
5. The simulation results for regional fiber deposition indicated that the depositions of small ellipsoids were highest in the larynx and the main nasal airway. The largest ellipsoidal fibers (fibers with $a = 10\ \mu m$, $\beta = 10$, and $a = 5\ \mu m$, $\beta = 25$ or larger), however, were

deposited mainly in the vestibule and the main nasal airway. Fine 5 μm ellipsoidal fibers or smaller could deposit in all parts of the upper airway, but as the fiber size increases, most particles are captured in the nasal valve.

6. The obtained results showed that for small ellipsoidal fibers the time variation of the deposition roughly follows the flow rate variation in the inhalation phase but with the increase of fiber size this trend is distorted. For larger ellipsoidal fibers, the transient deposition fraction sharply reaches to its maximum value shortly after the starting time of the inhalation phase (at about 10–40 percent of inhalation time).
7. The trend of time variation of the penetration of the ellipsoidal fibers to the lower airway had little or no correlation with the airflow rate variation. The maximum of the penetration for the small ellipsoidal fibers occurred almost in the middle of the accelerating phase of the inhalation period. Large ellipsoidal fibers, however, could hardly penetrate to the lower respiratory tract.

Appendix. -Validation

The validation of the user-defined functions for a single fiber was described by Tavakol et al. (2017). To verify the present user-defined functions for analyzing transport and deposition of fibrous particles, the predicted fiber deposition in a single nasal cavity used by Dastan et al. (2014) for the steady inhalation are compared with the results of previous computational and experimental studies in Fig. A1. Here IP denotes the impaction parameter, which is defined as,

$$IP = d^2_{eq} Q \tag{12}$$

where d_{eq} is the equivalent aerodynamic diameter used by Dastan et al. (2014) and Q is the air volume flow rate. Fig. A1 shows that the trends of different results are roughly the same, and the predictions of the present computational model are nearly the same as those of Dastan et al. (2014). It should point out that in the earlier study, an in-house code for solving the equations of translational and rotational motion of ellipsoids was used as a post-processor to ANSYS Fluent.

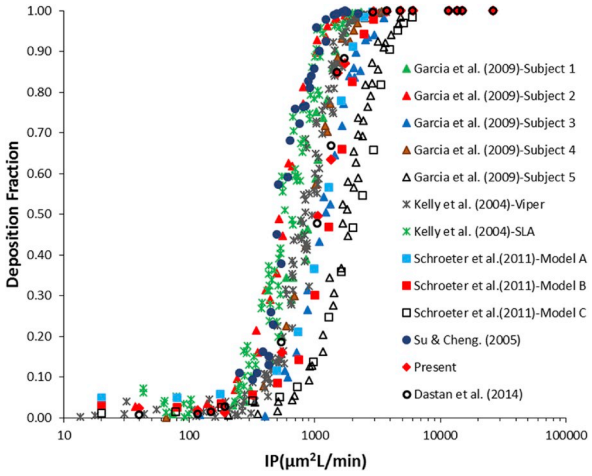

Fig. A1. Comparison of total fiber deposition fraction of the present study versus impaction parameter with the experimental and numerical results of earlier works.

References

Abouali, O., Keshavarzian, E., Ghalati, P. F., Faramarzi, A., Ahmadi, G., & Bagheri, M. H. (2012). Micro and nanoparticle deposition in human nasal passage pre and post virtual maxillary sinus endoscopic surgery. *Respiratory Physiology & Neurobiology, 181*(3), 335–345.

Ahmadi, G., & Abouali, O. (2017). Airflow and particle deposition in the upper respiratory airways. In E. E. Michaelides, C. T. Crowe, & J. D. Schwarzkopf (Eds.), *Multiphase flow handbook* (pp. 887–937). Boca Raton: CRC Press.

Asgharian, B., Owen, T. P., Kuempel, E. D., & Jarabek, A. M. (2018). Dosimetry of inhaled elongate mineral particles in the respiratory tract: The impact of shape factor. *Toxicology and Applied pharmacology, 361*, 27–35.

Bahmanzadeh, H., Abouali, & Ahmadi, G. (2016). Unsteady particle tracking of micro-particle deposition in the human nasal cavity under cyclic inspiratory flow. *Journal of Aerosol Science, 101*, 86–103.

Bahmanzadeh, H., Abouali, O., Faramarzi, M., & Ahmadi, G. (2015). Numerical simulation of airflow and micro-particle deposition in human nasal airway pre-and post-virtual sphenoidotomy surgery. *Computers in Biology and Medicine, 61*, 8–18.

Dastan, A., & Abouali, O. (2013). Microfiber motion and web formation in a microchannel heat sink: A numerical approach. *Computers & Fluids, 71*, 28–40.

Dastan, A., Abouali, O., & Ahmadi, G. (2014). CFD simulation of total and regional fiber deposition in human nasal cavities. *Journal Of Aerosol Science, 69*, 132–149.

Dong, J., Ma, J., Shang, Y., Inthavong, K., Qiu, D., Tu, J., et al. (2018). Detailed nanoparticle exposure analysis among human nasal cavities with distinct vestibule phenotypes. *Journal of Aerosol Science, 121*, 54–65.

Edgar, L. Y., Matida, A., & Johnson, M. R. (2010). Experimental measurements and computational modeling of aerosol deposition in the Carleton-Civic standardized human nasal cavity. *Journal of Aerosol Science, 41*, 569–586.

Fan, F., & Ahmadi, G. (1995). A sublayer model for wall deposition of ellipsoidal particles in turbulent streams. *Journal of Aerosol Science, 26*, 831–840.

Fan, F., & Ahmadi, G. (1995). Dispersion of ellipsoidal particles in an isotropic pseudo-turbulent flow field. *Fluids Engineering, 117*, 154–161.
Farhadi Ghalati, P., Keshavarzian, E., Abouali, O., Faramarzi, A., Tu, J., & Shakibafard, A. (2012). Numerical analysis of micro and nano-particle in a realistic human upper airway. *Computers in Biology and Medicine, 42*, 39–49.
Farkas, Á., Lizal, F., Elcner, J., Jedelsky, J., & Jicha, M. (2019). Numerical simulation of fiber deposition in oral and large bronchial airways in comparison with experiments. *Journal of Aerosol Science, 136*, 1–14.
Feng, Y., & Kleinstruer, C. (2013). Analysis of non-spherical particle transport in complex internal shear flows. *Physics of Fluids, 25*, 9001904.
Fenoglio, I., Aldieri, E., Gazzano, E., Cesano, F., Colonna, M., Scarano, D., et al. (2011). Thickness of multiwalled carbon nanotubes affects their lung toxicity. *Chemical Research in Toxicology, 25*, 74–82.
Garcia, G. J., Tewksbury, E. W., Wong, B. A., & Kimbell, J. S. (2009). Interindividual variability in nasal filtration as a function of nasal cavity geometry. *Journal of Aerosol Science Medicine and Pulmonary Drug Delivery, 22*, 139–155.
Ghahramani, E., Abouali, O., Emdad, H., & Ahmadi, G. (2014). Numerical analysis of stochastic dispersion of micro-particles in turbulent flows in a realistic model of human nasal/upper airway. *Journal of Aerosol Science, 67*, 188–206.
Grgic, B., Martin, A., & Finlay, W. (2006). The effect of unsteady flow rate increase on in vitro mouth–throat deposition of inhaled boluses. *Journal of Aerosol Science, 37*(10), 1222–1233.
Haghnegahdar, A., Zhao, J., & Feng, Y. (2019). Lung aerosol dynamics of airborne influenza A virus-laden droplets and the resultant immune system responses: An in silico study. *Journal of Aerosol Science, 134*, 34–55.
Häußermann, S., Bailey, A. G., Bailey, M. R., Etherington, G., & Youngman, M. (2002). The influence of breathing patterns on particle deposition in a nasal replicate cast. *Journal of Aerosol Science, 33*, 923–933.
Hörschler, I., Schröder, W., & Meinke, M. (2010). On the assumption of steadiness of nasal cavity flow. *Journal of Biomechanics, 43*(6), 1081–1085.
Inthavong, K., Wen, J., Tian, Z., & Tu, J. Y. (2008). Numerical study of fibre deposition in a human nasal cavity. *Journal of Aerosl Science, 39*, 253–265.
Kelly, J. T., Asgharian, B., Kimbell, J. S., & Wong, B. A. (2004). Particle deposition in human nasal airway replicas manufactured by different methods. Part I: Inertial regime particles. *Aerosol Science and Technology, 38*, 1063–1071.
Kesavanathan, J., Bascom, R., & Swift, D. L. (1998). The effect of nasal passage characteristics on particle deposition. *Journal of Aerosol Medicine, 11*, 27–39.
Moghadas, H., Abouali, O., Faramarzi, A., & Ahmadi, G. (2011). Numerical investigation of septal deviation effect on deposition of nano/microparticles in human nasal passage. *Respiratory Physiology & Neurobiology, 177*(1), 9–18.
Naseri, A., Abouali, O., & Ahamdi, G. (2017). Numerical analysis of stochastic dispersion of microparticles in turbulent natural convection flows around realistic model of human. *Building and Environment, 118*, 159–172.
Naseri, A., Abouali, O., Ghalati, P. F., & Ahmadi, G. (2014). Numerical investigation of regional particle deposition in the upper airway of a standing male mannequin in calm air surroundings. *Computers in Biology and Medicine, 52*, 73–81.
Naseri, A., Shaghaghian, S., Abouali, O., & Ahamdi, G. (2017). Numerical investigation of transient transport and deposition of microparticles under unsteady inspiratory flow in human upper airways. *Respiratory Physiology & Neurobiology, 244*, 56–72.
Nikookar, H., Abouali, O., Eghtesad, M., Sadrizadeh, S., & Ahamdi, G. (2019). Enhancing drug delivery to human trachea through oral airway using magnetophoretic steering of microsphere carriers composed of aggregated superparamagnetic nanoparticles and nanomedicine: A numerical study. *Journal of Aerosol Science, 127*, 63–92.
Ouchene, R., Khalij, M., Tanière, A., & Arcen, B. (2015). Drag, lift and torque coefficients for ellipsoidal particles: From low to moderate particle Reynolds numbers. *Computers & Fluids, 113*, 53–64.
Shanley, K. T., Zamankhan, P., Ahmadi, G., Hopke, P. K., & Cheng, Y.-S. (2008). Numerical simulations investigating the regional and overall deposition efficiency of the human nasal cavity. *Inhalation Toxicology, 20*(12), 1093–1100.
Shi, H., Kleinstreuer, C., & Zhang, Z. (2006). Laminar airflow and nanoparticle or vapor deposition in a human nasal cavity model. *Journal of Biomechanical Engineering, 128*(5), 697–706.
Smith, S., Cheng, Y. S., & Yeh, H. C. (2001). Deposition of ultrafine particles in human tracheobronchial airways of adults and children. *Aerosol Science and Technology, 35*, 697–709.
Su, W. C., & Cheng, Y. S. (2005). Deposition of fiber in the human nasal airway. *Aerosol Science and Technology, 39*, 888–901.
Tavakol, M. M., Ghahramani, E., Abouali, O., Yaghoubi, M., & Ahmadi, G. (2017). Deposition fraction of ellipsoidal fibers in a model of human nasal cavity for laminar and turbulent flows. *Journal of Aerosol Science, 113*, 52–70.
Tavakoli, B., Abouali, O., Bagheri, M. H., Yazdi, M., & Ahmadi, G. (2012). Micro particles transport and deposition in realistic geometry of human upper airways. *IJE Trans, 25(4)*, 315–322.
Tian, L., & Ahmadi, G. (2013). Fiber transport and deposition in human upper tracheobronchial airways. *Journal of Aerosol Science, 60*, 1–20.
Tian, L., Ahmadi, G., Wang, Z., & Hopke, P. K. (2012). Transport and deposition of ellipsoidal fibers in low Reynolds number flow. *Journal of Aerosol Science, 45*, 1–18.
Wang, Z., Hopke, P. K., Ahmadi, G., Cheng, Y. S., & Baronc, P. A. (2008). Fibrous particle deposition in human nasal passage: The influence of particle length, flow rate, and geometry of nasal airway. *Journal of Aerosl Science, 39*, 1040–1054.
Zamankhan, P., Ahmadi, G., Wang, Z., Hopke, P. K., Cheng, Y.-S., Su, W. C., et al. (2006). Airflow and deposition of nano-particles in a human nasal cavity. *Aerosol Science and Technology, 40*(6), 463–476.
Zhang, Z., Kleinstreuer, C., & Kim, C. (2002). Cyclic micron-size particle inhalation and deposition in a triple bifurcation lung airway model. *Journal of Aerosol Science, 33*(2), 257–281.
Zhao, J., Feng, Y., Bezerra, M., Wang, J., & Sperry, T. (2019). Numerical simulation of welding fume lung dosimetry. *Journal of Aerosol Science, 135*, 113–129.
Zhou, Y., & Cheng, Y. S. (2005). Particle deposition in a cast of human tracheobronchial airways. *Aerosol Science and Technology, 39*, 492–500.
Zhou, Y., Su, W. C., & Cheng, Y. S. (2008). Fiber deposition in the tracheobronchial region: Deposition equations. *Inhalation Toxicology, 20*(13), 1191–1198.